RSC Advances

PAPER

View Article Online
View Journal | View Issue

Cite this: *RSC Adv.*, 2023, **13**, 4656

Wrapping silicon microparticles by using well-dispersed single-walled carbon nanotubes for the preparation of high-performance lithium-ion battery anode†

Youngseul Cho,[a] Kyu Sang Lee,[b] Shuqing Piao,[b] Taek-Gyoung Kim,[c] Seong-Kyun Kang,[c] Sang Yoon Park,[d] Kwanghyun Yoo *[c] and Yuanzhe Piao *[abd]

Silicon microparticles (SiMPs) show considerable promise as an anode material in high-performance lithium-ion batteries (LIBs) because of their low-cost starting material and high capacity. The failure issues associated with the intrinsically low conductivity and significant volume expansion of Si have largely been resolved by designing silicon/carbon composites using carbon nanotubes (CNTs). The CNTs are important in terms of stress dissipation and the conductive network in Si/CNT composites. Here, we synthesized a SiMP/2D CNT sheet wrapping composite (SiMP/CNT wrapping) *via* a facile freeze-drying method with the use of highly dispersed single-walled CNTs. In this work, the well-dispersed CNTs are easily mixed with Si, resulting in effective CNT wrapping on the SiMP surface. During freeze-drying, the CNTs are self-assembled into a segregated 2D CNT sheet morphology *via* van der Waals interactions. The resulting CNT wrapping shows a unique wide range of conductive networks and mesh-like CNT sheets with void spaces. The SiMP/CNT wrapping 9 : 1 electrode exhibits good rate and cycle performance. The first charge/discharge capacity of SiMP/CNT wrapping 9 : 1 is 3160.7 mA h g^{-1}/3469.1 mA h g^{-1} at 0.1 A g^{-1} with superior initial coulombic efficiency of 91.11%. After cycling, the SiMP/CNT wrapping electrode shows good structural integrity with preserved electrical conductivity. The superior electrochemical performance of the SiMP/CNT wrapping composite can be explained by an extensive conductive CNT network on the SiMPs and facile lithium-ion diffusion *via* mesh-like CNT wrapping.

Received 23rd November 2022
Accepted 21st January 2023

DOI: 10.1039/d2ra07469a

rsc.li/rsc-advances

1. Introduction

The ever-growing demand for lithium-ion batteries with high energy densities, especially batteries for promising advanced mobile electronics and electrical vehicles, has been confronted by the battery community.[1–3] Silicon (Si) anodes are considered one of the promising anode materials for next-generation lithium-ion batteries (LIBs) due to their superior theoretical specific capacity (>4000 mA h g^{-1}) and low working potential (~0.3 V *vs.* Li/Li^+).[1,2,4] To be specific, cost-effective micron-scale silicon could become more competitive in future research work and applications.[4–6] However, the high capacity of Si, which originates from the alloying mechanism, introduces the failure mechanisms of active material pulverization (~300%), electrode delamination, and continuous solid electrolyte interphase (SEI) layer growth.[1,2] Furthermore, another critical problem of Si anodes is their intrinsically low electrical conductivity (~10^{-3} S m^{-1}).[2] To address these issues, several composite designs have been reported to enhance the electrochemical performance of Si anodes.[5–7]

The preparation of silicon-based composites combined with carbonaceous materials imparts valuable properties to Si, whereby the challenges of huge volume expansion and poor electronic conductivity can be simultaneously resolved.[3,6,8,9] Among the various carbon materials, carbon nanotubes (CNTs) have received extensive consideration in the targeting of efficient composite design.[10–13] From a structural viewpoint, the superb mechanical stabilities and excellent electrical conductivities of CNTs have been reported to overcome the aforementioned intrinsic issues of Si electrodes.[14–16] Despite the impressive advances, Si/CNT composite design typically

[a]*Program in Nano Science and Technology, Graduate School of Convergence Science and Technology, Seoul National University, 145 Gwanggyo-ro, Yeongtong-gu, Suwon-Si, Gyeonggi-do, 16229, Republic of Korea. E-mail: parkat9@snu.ac.kr*

[b]*Department of Applied Bioengineering, Graduate School of Convergence Science and Technology, Seoul National University, 145 Gwanggyo-ro, Yeongtong-gu, Suwon-Si, Gyeonggi-do, 16229, Republic of Korea*

[c]*BETTERIAL Co., 307, 52, Sagimakgol-ro, Jungwon-gu, Seongnam-si, Gyeonggi-do, Republic of Korea. E-mail: kyoo@betterial.io*

[d]*Advanced Institutes of Convergence Technology, 145 Gwanggyo-ro, Yeongtong-gu, Suwon-si, Gyeonggi-do, 16229, Republic of Korea*

† Electronic supplementary information (ESI) available: Fig. S1–S9, eqn (S1), Tables S1 and S2 as described in the manuscript. See DOI: https://doi.org/10.1039/d2ra07469a

requires complicated procedures.[17–19] Furthermore, the intrinsic properties of CNT, such as severe entanglement and agglomeration owing to π–π interactions and van der Waals forces, are recognized as critical drawbacks.[13,14] The CNT distribution is an important factor to dissipate Si volume changes and generate a well-dispersed conductive network. Recently, CNT dispersions have been introduced as a conductive additive in a wide range of micron-scale active material particles, including silicon microparticles (SiMPs).[14] The resulting segregated CNT network in the electrode could improve both the mechanical properties and electrical conductivity with low charge-transfer resistance. For this reason, it is highly desirable to further develop a Si/CNT composite by taking advantage of its structural properties. According to previous studies, the carbon wrapping structure of Si/C composites was also found to effectively mitigate volume changes of Si and promote extensive conductive networks.[9,20]

For this reason, herein, we prepared a SiMP/2D CNT sheet wrapping composite (SiMP/CNT wrapping) *via* freeze-drying by using highly dispersed single-walled CNTs. Lyophilization is one of the widely used methods for composite preparation in energy storage systems.[21–23] During freeze-drying, the well-dispersed CNT networks are simply self-assembled into segregated CNT sheets, resulting in efficient wrapping on SiMPs. In particular, the CNT dispersion formed a unique CNT sheet morphology without agglomeration of the CNTs. In addition, the well-dispersed CNTs are easily mixed with the SiMPs in the preparation step. The optimized structural properties of the SiMP/CNT wrapping composite were investigated by controlling the weight ratios between SiMP and CNT. The thickness of the CNT wrapping sheet can be varied with the amount of CNT dispersion. The resulting SiMP/CNT wrapping composite was tested as an anode material in lithium-ion batteries. The optimized SiMP/CNT wrapping 9 : 1 composite exhibits superior rate and cycling performance with high capacities. In addition, the SiMP/CNT wrapping 9 : 1 electrode shows high initial and later-cycle coulombic efficiencies, implying stable SEI formation and the structural integrity of the composite. The as-synthesized SiMP/CNT wrapping composite has multiple attractive advantages. The tight CNT wrapping on the SiMPs could alleviate the volume expansion of Si and preserve electrical conductivity during repeated charge and discharge cycles. Furthermore, the mesh-like CNT sheets composed of 1D CNTs are expected to offer a wide range of extensive conductive networks and facile lithium-ion diffusivity, which endow SiMP with electrochemical activity upon cycling. This work provides useful guidelines for SiMP/CNT composite design using well-dispersed CNTs and suggests the easy preparation of a segregated 2D CNT wrapping network *via* lyophilization.

2. Experimental

2.1 Materials

Silicon microparticles (1–5 microns, 99.9%, metal basis) were purchased from Alfa Aesar. Sodium carboxymethyl cellulose (CMC, Average M.W. = 700 000) was purchased from Sigma-Aldrich. A conductive additive (Super P) was purchased from Timcal company (Switzerland). Single-walled carbon nanotube aqueous dispersion (SWCNT, 0.4 wt%) was purchased from Betterial Co. (SWCNT dispersion (S1304WK, BETTERIAL Co., Ltd., Korea)).

2.2 Preparation of oven-dried CNT dispersion, freeze-dried CNT dispersion, and freeze-dried pristine SWCNT powder

For the oven-dried CNT dispersion sample, the CNT dispersion was poured into a disposable plastic weighing dish. Next, the CNT dispersion was fully dried at 50 °C for 12 hours using a convection oven. The freeze-dried CNT dispersion was prepared *via* a lyophilization method. The CNT dispersion (3 g) was poured into a Falcon tube and mixed with DI water (1 mL). The capacity of the Falcon tube was 15 mL. Next, the resulting mixture was frozen in a liquid nitrogen bath and freeze-dried for 2 days. The pristine SWCNT powder was mixed with DI water and freeze-dried for 2 days.

2.3 Preparation of active material – silicon microparticle/2D carbon nanotube sheet wrapping composite (SiMP/CNT wrapping)

For the SiMP/CNT wrapping 9 : 1 composite, silicon microparticles (0.18 g) were first mixed with DI water (5 mL) using a Falcon tube. The capacity of the Falcon tube was 50 mL. The aqueous SiMP mixture was sonicated for 5 minutes. After sonication for 5 minutes, 2 g of CNT dispersion was added to the SiMP aqueous dispersion. For freeze-drying, 500 mL of liquid nitrogen was poured into a thermos with a 2 L capacity. Next, a 50 mL Falcon tube filled with the SiMP/CNT dispersion mixture was gripped using a laboratory tong. The Falcon tube was suddenly placed in the liquid nitrogen bath in the thermos. Upon freezing for 5 minutes, the entire Falcon tube should be immersed in liquid nitrogen and the Falcon should be held by tongs so that it stands upright. After freezing, the screw-top of the Falcon tube was opened and then covered with a piece of Kimwipe (small size, 107 mm × 210 mm) and sealing tape. The sealed Falcon tube was placed into a wide-mouth glass bottle in a freeze-dryer. Detailed information can be also found in the images in Fig. S1†. The sample was freeze-dried for 2 days. Next, the SiMP/CNT wrapping 8 : 2 composite was synthesized using the same method as for the preparation of the SiMP/CNT wrapping 9 : 1 composite, but with different amounts of SiMP particles and CNT dispersion (0.16 g and 4 g, respectively).

2.4 Preparation of silicon nanoparticle/carbon nanotube composite (SiNP/CNT)

A mixed solution of silicon nanoparticles (SiNP, 0.18 g), DI water (3 mL), and CNT dispersion (2 g) was prepared for the SiNP/CNT 9 : 1 composite under the same conditions as the SiMP/CNT composites. The resulting mixture was freeze-dried for 2 days. For the SiNP/CNT 8 : 2 composite, SiNP (0.16 g) was mixed with DI water (3 mL) and the CNT dispersion (2 g). The resulting mixture was freeze-dried using the same method as the SiNP/CNT 9 : 1 composite.

2.5 Material characterization

High-resolution transmission electron microscopy (HR-TEM) analysis was conducted using JEM-2100F (JEOL). Scanning electron microscopy (SEM) analysis with energy-dispersive X-ray spectroscopy (EDS) mapping was carried out using an S-4300SE FE-SEM (Hitachi). N_2 adsorption/desorption testing was conducted using an adsorption analyzer using BELSORP-max II (MictrotracBEL). X-ray diffraction (XRD) was done using a D8-Advance (XRD, a1 system) (BRUKER MILLER). Raman spectra were recorded using a DXR2xi spectrometer (Thermo) with an excitation wavelength of 532 nm. Thermogravimetric analysis (TGA) was carried out using a TGA/DSC 1 analyzer (Mettler Toledo).

2.6 Electrochemical characterization

Electrodes were fabricated by first preparing slurries consisting of the active material (SiMP/CNT wrapping composite), a conductive additive (Super P), and CMC binder (sodium carboxymethyl cellulose, CMC) in a weight ratio of 70 : 15 : 15 in DI water as the solvent. The as-prepared slurries were coated on the current collector (Cu foil) using a doctor blade and then dried in a vacuum oven at 60 °C for 4 hours. The electrode fabricated in our work was compared with that of other SiMP/carbon composite electrodes in Table S1†. The areal mass loading of the active material in the electrode was 0.7 mg cm^{-2}. Based on the comparison chart in Table S1†, the loading mass of the SiMP/CNT wrapping was comparable to that of other SiMP/carbon composite-based electrodes. A 2016-type coin cell was assembled in an Ar-filled glove box. The electrolyte was 1.3 M $LiPF_6$ dissolved in ethylene carbonate (EC)/diethyl carbonate (DEC) (3 : 7 vol/vol) with 10 wt% of fluoroethylene carbonate (FEC) (PANAX). The galvanostatic intermittent titration technique (GITT) was applied with a pulsed current (100 mA g^{-1}) for 30 min with rest intervals (2 hours). For the electrical impedance spectroscopy (EIS) test, a ZIVE SP1 (ZIVE lab) was used with a frequency range between 500 mHz and 10 kHz. For EIS analysis of the symmetric cells of a fresh electrode, an electrode disk with a circle shape with a diameter of 11 mm was cut in half. The half-cut electrodes were assembled into a symmetric cell in a glove box. The as-assembled symmetric cell was used for EIS analysis. After analysis, the symmetric cell was disassembled in the glove box and re-assembled as half-cells by using the half-cut electrodes as the working electrode and lithium metal as a counter electrode, respectively. After 20 cycles at 1 A g^{-1}, the half-cells were fully lithiated at a low current density of 0.2 A g^{-1}. Considering the lithiation capacity, each electrode was half-delithiated at the same current density to 50% of the state of charge (SoC). At ~50% SoC, the half-cells were disassembled and re-assembled as symmetric cells in the glove box. The as-assembled 20-cycle electrode symmetric cell with 50% SoC was further analyzed for internal resistance using EIS testing.

3. Results and discussion

Fig. 1a shows a schematic illustration of the preparation of the silicon microparticle/2D carbon nanotube sheet wrapping composite, which is denoted as SiMP/CNT wrapping. For the synthesis of the SiMP/CNT wrapping composite, SiMP particles (diameter of 1–5 μm) were first mixed with a certain amount of DI water and then added to a well-dispersed single-walled CNT dispersion (SWCNT dispersion). Next, the mixture was frozen in a liquid nitrogen bath and freeze-dried *via* the lyophilization method.[24,25] In detail, the lyophilization process consisted of two different steps: (1) freezing *via* ice crystal growth and (2) drying by ice sublimation.[24] During the freeze-drying process, the CNT networks in the mixture were self-assembled into segregated 2D CNT sheets. After the sublimation of the ice, the SiMP/CNT wrapping composites were obtained. In particular, the SiMPs were effectively encapsulated by the CNT wrapping

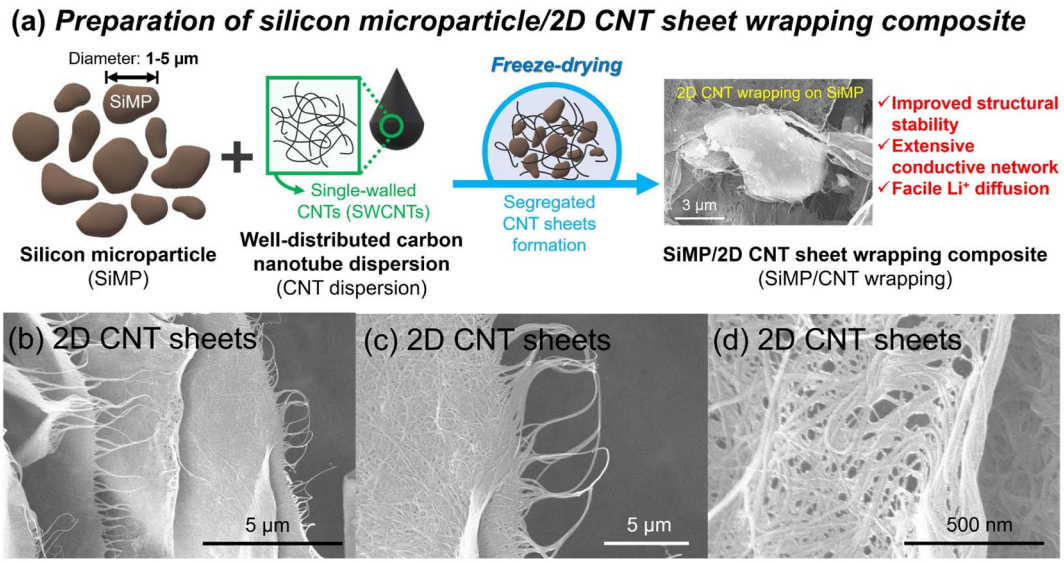

Fig. 1 (a) Schematic illustration of the preparation of the silicon microparticle/2D carbon nanotube (CNT) sheet wrapping composite (SiMP/CNT wrapping). SEM images of 2D CNT sheets at (b and c) low and (d) high magnification.

sheets in the composite. In Fig. 1b–d, the scanning electron microscopy (SEM) images exhibit thin 2D CNT sheets that were prepared *via* lyophilization using a CNT dispersion without SiMPs. As we freeze-dried the SWCNT dispersion, the resulting sample shows a unique 2D sheet structure composed of highly dispersed CNTs (Fig. 1b and c). We consider that the segregated CNT structure could be formed due to the self-assembly behavior of the components during the freeze-drying process and the strong van der Waals interaction between the SWCNTs. The SEM image with high magnification in Fig. 1d reveals a 2D SWCNT membrane structure with appropriate void spaces within the CNT sheets. With this unique structure in mind, we investigated the morphological features of CNT dispersions obtained with various preparation processes as described in the following paragraph.

Based on the unique CNT architecture in Fig. 1b–d, we further explored the well-dispersed CNTs and the effect of the preparation method on the structural properties of the CNTs. Fig. 2a shows SEM images of pristine SWCNT powder without any purification or chemical treatment. The severe CNT aggregation and strongly entangled CNTs in Fig. 2a could be due to intrinsic properties of the SWCNTs, such as van der Waals forces and strong π–π interactions.[26,27] The intrinsically strong aggregation of SWCNTs limits their application and usage in a wide range of research areas.[28,29] As shown in Fig. 2b and c, the SEM and transmission electron microscopy (TEM) images of the CNT dispersion display well-dispersed SWCNT networks without CNT bundle aggregates. For the SEM analysis, the CNT dispersion was dropped on a Cu foil and dried in a vacuum oven, which is the same as the electrode preparation in the experimental section. Furthermore, the dispersibility of the CNT dispersion was investigated, as shown in Fig. S2†. In Fig. S2a and b†, the digital photographs of the CNTs show highly dispersed SWCNTs. The uniform dispersion was easily

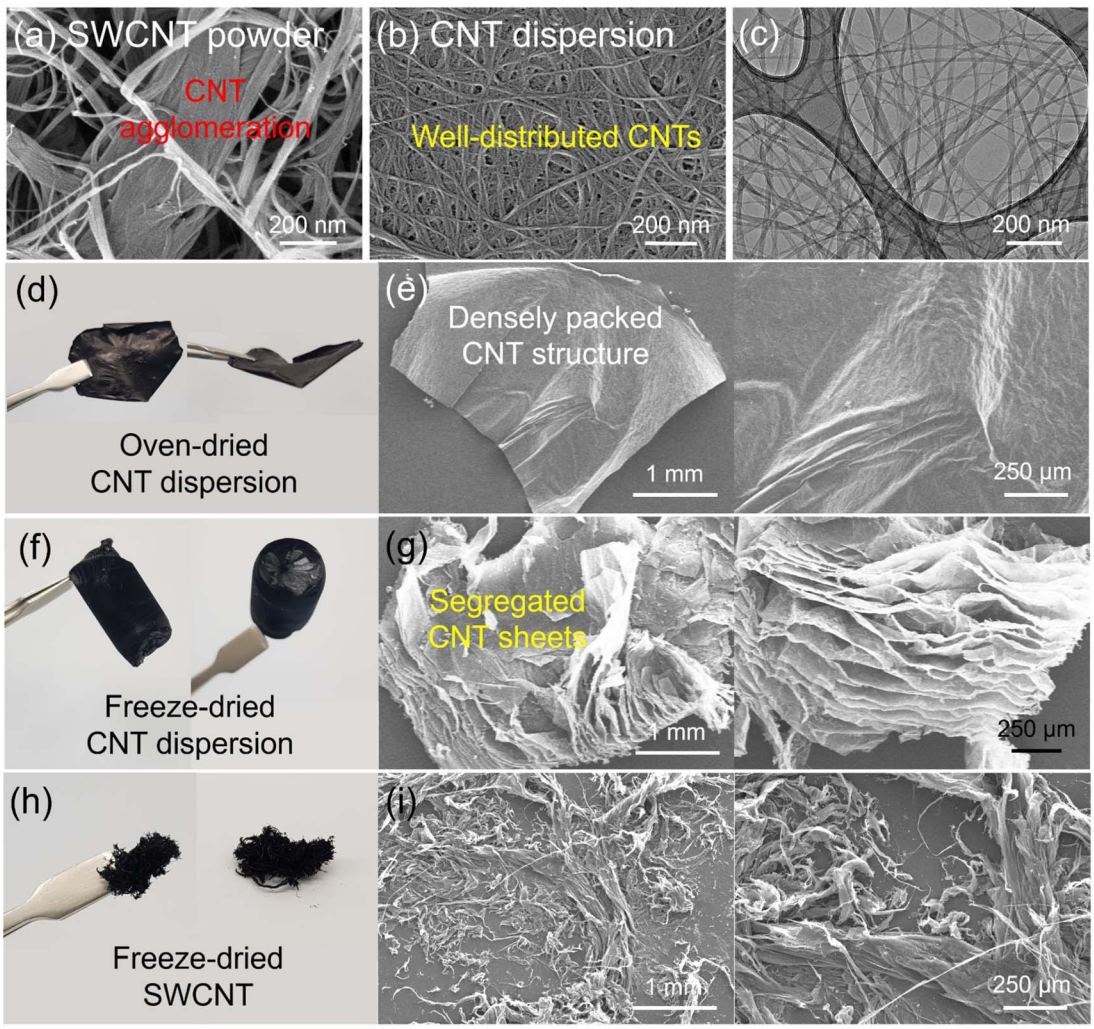

Fig. 2 Scanning electron microscopy (SEM) images of (a) pristine single-walled CNT (SWCNT) powder and (b) CNT dispersion. (c) Transmission electron microscopy (TEM) image of CNT dispersion. (d) Digital photographs of oven-dried CNT dispersion. (e) SEM images of oven-dried CNT dispersion with low and high magnification. (f) Digital photographs of freeze-dried CNT dispersion. (g) SEM images of freeze-dried CNT dispersion with low and high magnification. (h) Digital photographs of freeze-dried pristine CNTs. (i) SEM images of the freeze-dried pristine CNTs with low and high magnification.

observed with the naked eye. When it was applied to slide glass, the even coating of the SWCNT dispersion without aggregates indicated its superior dispersibility (Fig. S2c†). The dispersion stability of the CNT dispersion continued even after 24 hours (Fig. S2d and e†). Optical microscopy (OM) images of well-dispersed SWCNTs and pristine SWCNTs are shown in Fig. S2f and g†. Compared to the severely entangled CNT aggregates of the pristine SWCNT, the SWCNT dispersion exhibits good dispersion properties. Our approach to the preparation of the SiMP/CNT wrapping composites involved lyophilization of a mixed solution of SiMPs and the SWCNT dispersion. To determine the necessary experimental conditions to obtain the unique CNT architecture, we prepared CNT samples using an oven-drying or freeze-drying method. Detailed information about the preparation of the oven-dried and freeze-dried CNT samples is provided in the experimental section. As shown in Fig. 2d, the digital photograph of the oven-dried CNTs shows a dense CNT film. Accordingly, thick and closely packed CNT networks were observed in the SEM images of the oven-dried CNT sample (Fig. 2e). In contrast, the freeze-dried CNT dispersion sample exhibited different structural properties. The freeze-dried CNTs in Fig. 2f are similar to an aerogel structure. The 2D CNT structure composed of SWCNTs is shown in the SEM images of the freeze-dried CNT sample in Fig. 2g. From the structural view of the freeze-dried CNT sample, each CNT sheet was created in parallel to each other, indicating that self-assembly occurred during freeze-drying.[24,25] In addition, we consider that the segregated CNT network would be a result of the van der Waals interactions between CNTs.[12,14] Therefore, we speculate that the formation of thin 2D CNT sheets is provided by the chemical interaction between CNTs and the freeze-drying method. However, the segregated 2D CNT network was not formed when we freeze-dried aqueous pristine SWCNT powder dispersion due to severe aggregation between SWCNTs (Fig. 2h and i).

Hereafter, the SiMP/CNT wrapping 8 : 2 and SiMP/CNT wrapping 9 : 1 composite are denoted as 8 : 2 and 9 : 1 in figures and data. Fig. 3a and b shows SEM images of counterparts for SiMP/CNT wrapping composites such as SiMP and SWCNT sheets. The SEM image in Fig. 3a displays the irregular shape of pristine Si microparticles with a size range of around 1–5 microns. In Fig. 3b, extensive 2D CNT sheets were observed in the SEM image. Based on the unique CNT architecture in Fig. 1b–d, we prepared SiMP/CNT wrapping composites following the same synthetic route as for 2D SWCNT sheet fabrication. In Fig. 3c, the digital photograph of the freeze-dried SiMP/CNT wrapping 8 : 2 composite shows a dense aerogel structure. In an attempt to investigate the morphological and structural properties, we prepared SiMP/CNT wrapping composites with different weight ratios between the SiMPs and SWCNT dispersion. As shown in Fig. 3d and e, all the obtained SiMP/CNT wrapping composites with different weight ratios between SiMPs and CNTs show a unique 2D CNT sheet wrapping structure that is similar to that of the 2D CNT sheets (Fig. 3b). The result implies that the 2D SWCNT sheets are formed *via* freeze-drying even in the presence of SiMPs. Overall, the SiMPs are wrapped with a wide range of 2D CNT sheets, which were segregated and van der Waals-bonded SWCNT networks. High-magnification SEM images of SiMP/CNT wrapping 8 : 2 shows that the SiMP particles are effectively wrapped by a 2D CNT membrane (Fig. 3d). Even with a smaller SWCNT dispersion content, the resulting SiMP/CNT wrapping 9 : 1 composite also shows a similar CNT network but thin CNT sheet coverage on the SiMPs (Fig. 3e). The less-dense CNT sheet wrapping of the SiMP/CNT wrapping 9 : 1 composite could be due to the lower amount of SWCNT dispersion. With increased content of SWCNT dispersion, the resulting SiMP/CNT wrapping 8 : 2 sample maintained the extensive CNT wrapping network; however, thicker 2D CNT sheets were formed. This demonstrates that the changes in the content of the components could affect the resulting structure of the SiMP/CNT wrapping composite.[30] Since the 2D CNT sheets effectively wrapped the SiMPs, we further estimated that the 2D SWCNT sheets, which consist of mechanically strong SWCNTs, could act as an efficient buffer matrix inside the composite for preserving its structural integrity against the huge volume changes of Si.[14] Fig. 3f shows a digital photograph of an aqueous mixture of SiMPs and CNTs. Compared to the pristine SWCNTs, the CNT dispersion + SiMP mixture exhibits good dispersion without severe aggregation of the CNTs. The well-mixed CNT dispersion + SiMP could ensure CNT distribution in the composite, resulting in effective Si volume change dissipation and an evenly dispersed conductive network. As shown in Fig. 3f, a digital photograph of the freeze-dried SiMP/pristine SWCNT composite shows a powder-type sample. To investigate the distribution of SiMP and CNT in the composite, we conducted SEM analysis with energy-dispersive X-ray spectroscopy (EDS) mapping. Compared to the aggregated CNT networks in the SiMP/pristine SWCNT composite, the SiMP/CNT wrapping 9 : 1 composite shows extensive 2D CNT wrapping on the SiMPs (Fig. 3g and h). To further investigate the morphological features of the self-assembled 2D CNT wrapping network formation, the effect of the silicon particle size and weight ratio between silicon and the CNT dispersion on the Si/CNT composite were tested, as shown in Fig. 3i, S3 and S4†. Therefore, we also prepared a Si/CNT composite using silicon nanoparticles with a diameter of 50 nm with different weight ratios between the SiNP powder and SWNCT dispersion. According to previous studies, there was a prerequisite that the particles should be micron-sized to form a segregated CNT network.[12,14] However, the effective hierarchical CNT network was simply formed when we freeze-dried well-dispersed CNTs (Fig. 3b). For the micron-scale Si, 2D CNT wrapping is formed on the SiMPs, and the CNT wrapping thickness can be varied by controlling the CNT content. Compared to the SiMP/CNT sample (Fig. 3c), the digital photograph of the freeze-dried SiNP/CNT composite exhibits a loosely interconnected aerogel structure, which might be due to the larger surface area of the silicon nanoparticles. Although the SiNP/CNT 9 : 1 composite shows a non-segregated structure (Fig. S3†), an increased amount of CNTs results in the formation of embedded SiNPs in a micro-scroll CNT structure *via* freeze-drying (Fig. 3i and S4†).[10] During the freeze-drying, the well-dispersed CNT could form a 2D assembly even with nanosized silicon particles. This result provides a guideline to

develop segregated 2D CNT network-based Si composites by selecting different sizes of silicon particles or adjusting the proportion between Si and well-dispersed SWCNTs.

To characterize their structural properties, detailed analyses were conducted of the SiMP, SWCNT dispersion, and SiMP/CNT wrapping composites. Due to the liquid-type property of the

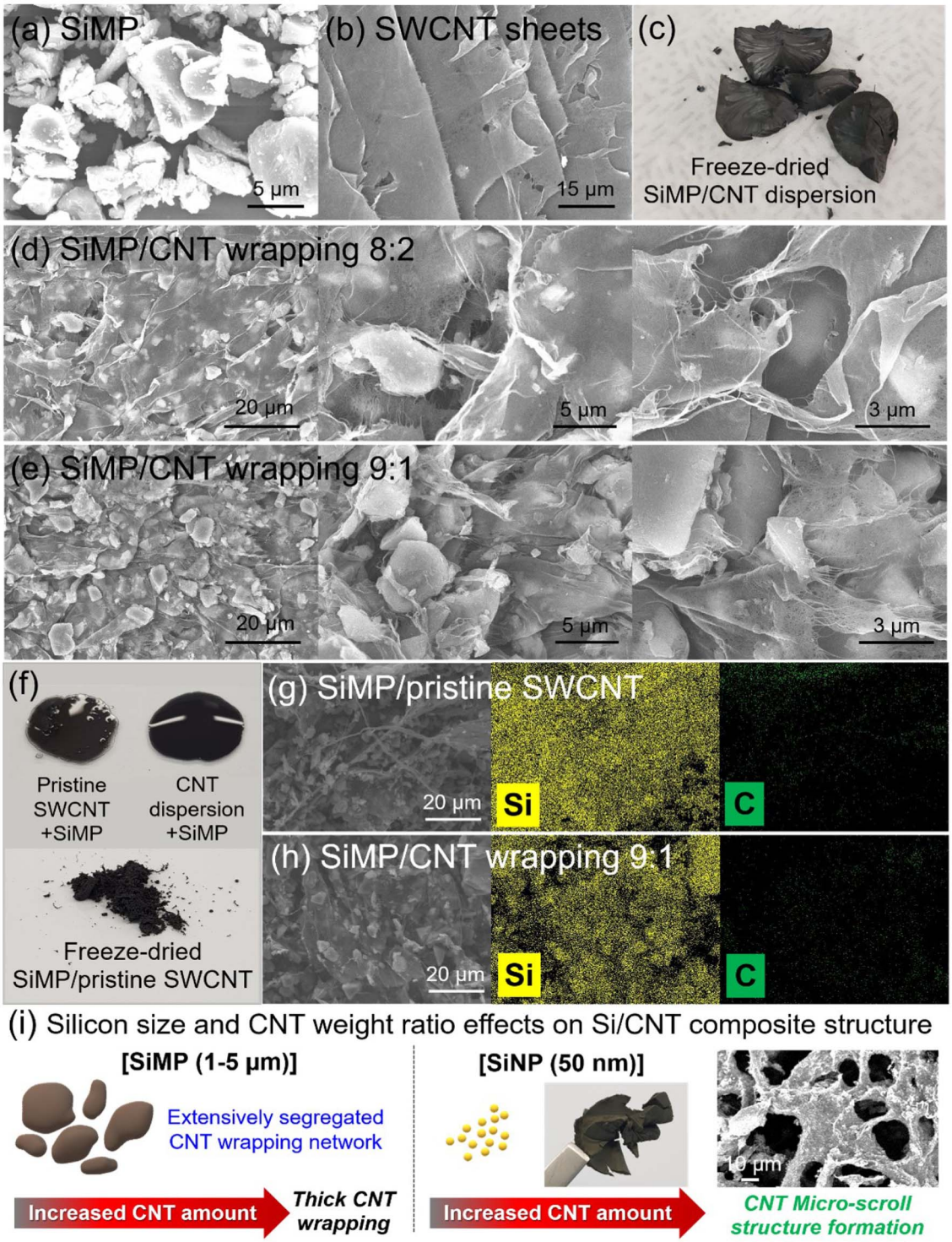

Fig. 3 SEM image of (a) SiMP and (b) SWCNT sheets at low magnification. (c) Digital photograph of the SiMP/CNT wrapping 8 : 2 composite after freeze-drying. SEM images of (d) the SiMP/CNT wrapping 8 : 2 composite and (e) SiMP/CNT wrapping 9 : 1 composite at low and high magnification. (f) Comparison between the aqueous mixture of pristine SWCNT + SiMP and CNT dispersion + SiMP samples, and a digital photograph of the freeze-dried SiMP/pristine SWCNT composite. SEM image of (g) SiMP/pristine SWCNT and (h) SiMP/CNT wrapping 9 : 1 composite with EDS mapping. (i) Effects of the silicon particle size and the weight ratio between Si and SWCNT dispersion on the Si/CNT composite structure.

SWCNT dispersion, the SWCNT dispersion was freeze-dried for material characterization. As shown in Fig. 4a, the sharp peak in the Raman spectrum of SiMP at around 500 cm-1 corresponds to crystalline Si.[4,31] In addition, the SWCNTs show a Raman spectrum with distinctive peaks. The peaks at the low wavenumber side at around 1350 cm^{-1} and at around 1590 cm^{-1} are derived from the radial breathing mode (RBM), defect, and in-plane vibration of a six-membered ring of carbon materials, respectively.[32] According to previous research, SWCNTs shows splitting of the G band into G+ and G−, which are referred to as the longitudinal wave mode and transverse wave mode perpendicular to the axis.[33] In Fig. 4a, the Raman spectra of the SiMP/CNT wrapping 9 : 1 and SiMP/CNT wrapping 8 : 2 composites show specific peaks of SiMPs and SWCNTs. The result implies the co-existence of both SiMPs and SWCNTs in the SiMP/CNT wrapping composites. Interestingly, the SiMP/CNT wrapping composites show pronounced peaks from SWCNT but a weak Si peak. We consider that this result could be due to efficient SWCNT wrapping on the SiMPs. Compared to SiMP/CNT wrapping 8 : 2 composite, the SiMP/CNT wrapping 9 : 1 composite exhibits a greater intensity for the crystalline silicon peak around 500 cm^{-1} due to the larger amount of SiMP in the composite. The X-ray diffraction (XRD) pattern in Fig. 4b shows the characteristic crystalline peaks in the SiMP/CNT wrapping composites. The XRD peaks in the SiMP/CNT wrapping composites correspond to the XRD patterns of the SiMPs and SWCNTs.[34,35] Specifically, the XRD patterns of the SiMPs can be indexed to Si (JCPDS 27-1402).[34,36] Based on the XRD data, the SiMP/CNT wrapping composites exhibit noticeable SiMP peaks but show weak SWCNT peaks. The weak intensity of the SWCNT peaks could be due to the low amount of SWCNTs in the SiMP/CNT wrapping composites. To investigate the SWCNT content in the SiMP/CNT wrapping composite material, thermogravimetric analysis (TGA) analysis was conducted (Fig. 4c). Each sample was heated to 900 °C under air atmospheric conditions with a ramp rate of 10 °C min^{-1}. Due to the oxidation of silicon at high temperatures in the air atmosphere, TGA curves of SiMP, SiMP/CNT wrapping 9 : 1, and SiMP/CNT wrapping 8 : 2 show gradual weight increases.[11,37,38] In Fig. 4c, the TGA curves indicate that the amount of SWCNTs in the SiMP/CNT wrapping 8 : 2 and SiMP/CNT wrapping 9 : 1 composites is 16.9% and 8.7%, respectively. Accordingly, the SiMP content in SiMP/CNT wrapping 8 : 2 and SiMP/CNT wrapping 9 : 1 was estimated to be 83.1% and 91.3%, respectively. It can be seen that the amount of SWCNTs in SiMP/CNT wrapping 8 : 2 is about twice that in SiMP/CNT wrapping 9 : 1. Fig. 4d shows the N2 isotherm plots of SiMP, SWCNT, and SiMP/CNT wrapping composites along with their Brunauer–Emmett–Teller (BET) surface areas. The SiMP, SWCNT, SiMP/CNT wrapping 8 : 2, and SiMP/CNT wrapping 9 : 1 composite exhibit surface areas of 5.85, 39.55, 12.24, and 8.24 $m^2\ g^{-1}$, respectively. Although both SiMP/CNT wrapping 8 : 2 and SiMP/CNT wrapping 9 : 1 show similar composite structures (Fig. 3d and e), they exhibit different BET surface areas. It can be found that the addition of a larger amount of SWCNTs results in a BET surface area increase. We consider that the increased content of mesh-like 2D CNT sheets in the SiMP/CNT wrapping composite could generate a larger surface area. In Fig. 4e, the Barrett–Joyner–Halenda (BJH) pore distribution data show that the SWCNTs have large pore volumes and a wide range of pore sizes. This result is consistent with the unique structure of the 2D CNT sheets in Fig. 1b–d. The segregated CNT network with inner voids between junctions and CNTs could affect the large pore volumes. With increasing SWCNT content, the SiMP/CNT

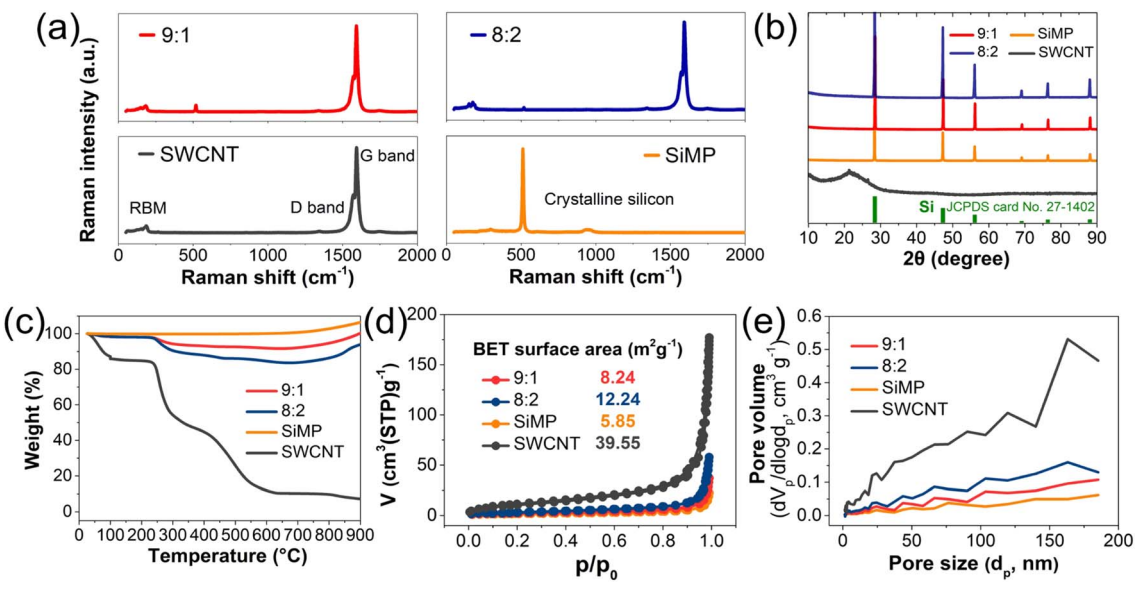

Fig. 4 (a) Raman spectra and (b) X-ray diffraction (XRD) patterns of SiMP/CNT wrapping 9 : 1, SiMP/CNT wrapping 8 : 2, SWCNT, and SiMP. (c) Thermogravimetric analysis (TGA) curves of SiMP/CNT wrapping 9 : 1, SiMP/CNT wrapping 8 : 2, SWCNT, and SiMP. The TGA analysis was conducted in an air atmosphere up to 900 °C (ramping rate of 10 °C min^{-1}). (d) N_2 adsorption–desorption isotherm plots with BET surface area and (e) BJH pore distribution of SiMP/CNT wrapping 9 : 1, SiMP/CNT wrapping 8 : 2, SWCNT, and SiMP.

wrapping composite displays a larger pore volume. The BET and BJH data are correlated with the morphological features of SiMP/CNT wrapping composites in Fig. 3d and e. Based on the results, we expected that the well-dispersed SWCNT content in the SiMP/CNT wrapping composites could strongly affect structural properties such as surface areas and porosity.

Each SiMP/CNT wrapping electrode was prepared using active material (SiMP/CNT wrapping):conductive additive (Super P):binder (CMC) in a weight ratio of 70 : 15 : 15. The electrochemical performances of the SiMP/CNT wrapping electrodes were evaluated in a galvanostatic mode in the potential range from 0.01 to 1.5 V *versus* Li/Li^+. The SiMP/CNT wrapping electrode was fabricated in a half-cell configuration with lithium metal. Before the electrochemical test, the morphology and structure of the SiMP/CNT wrapping composite electrodes were investigated. The SEM images of the SiMP/CNT wrapping electrodes in Fig. S5† show the original structure of the active material, implying the structural stability of the SiMP/CNT wrapping after electrode fabrication. Generally, silicon electrodes are fabricated using an active material, a conductive additive, and a polymeric binder. In particular, the conductive additive plays an important role in providing a continuous conductive network within the electrode and improving the intrinsically low conductivity of silicon. In addition, in recent studies of Si/C composites, electrodes have also been prepared using a certain amount of conductive additive (Table S1†). As we used a conductive additive for the electrode fabrication, the resulting electrode exhibits a hybrid conductive network, which consists of carbon spheres and CNTs. The Super P particles are distributed with the SiMP/CNT wrapping composite in the electrode. When the SWCNT content was increased, the resulting SiMP/CNT wrapping 8 : 2 generated thick SWCNT coverage in the electrode (Fig. S5a and b†). Due to the larger amount of SWCNTs in the SiMP/CNT wrapping 8 : 2 composite, denser CNT networks were observed in the high-magnification SEM image in Fig. S5c†. However, the SEM image of the SiMP/CNT wrapping 9 : 1 composite-based electrode in Fig. S5d† shows a thinner 2D CNT wrapping network. Along with the mesh-like CNT sheets, the silicon microparticles underneath the CNT sheets were also observed. The result implies that the smaller amount of CNT dispersion generates porous CNT membranes, not dense CNT coverage, at the electrode level. The voids inside the electrode seem to decrease with increasing the amount of SWCNT dispersion in the composite. As a result, we consider that the SiMP/CNT wrapping composite structure could affect the electrode architecture. Additionally, this could be reasonable considering that the increased porosity in the electrode could facilitate inner void space toward volume changes of Si and accommodate facile lithium-ion diffusion in it.[9]

To investigate the electrochemical stability of the SWCNT dispersion, cyclic voltammetry (CV) of the SWCNT dispersion-coated electrode was conducted in a potential range of 0.01–3.0 V *versus* Li/Li^+ (Fig. 5a). Fig. 5a shows the CV profile of the SWCNT dispersion, which lacks distinct redox peaks. The peaks in the potential range in the blue square box are related to the decomposition of electrolytes in the first cycle, which is usually observed in Si-based anode materials. Based on the weaker current response of the peaks, we considered the SWCNT dispersion to be suitable for the electrochemical test. In Fig. 5b and S6†, the CV curves of the SiMP/CNT wrapping 9 : 1 and SiMP/CNT wrapping 8 : 2 electrodes are shown. The CV analysis was conducted at the same scan rate of 0.2 mV s^{-1} for 5 cycles. The distinct anodic and cathodic peaks of Si are observed.[3,4,39,40] In detail, the cathodic peaks around 0.2 and 0.01 V correspond to the lithiation of Si.[9] In the anodic scan, two peaks at around 0.3 and 0.5 V are related to the de-lithiation process from the Li–Si alloy to amorphous silicon.[39,41] The increase in the magnitude of the current peaks with subsequent scan cycles could be due to an Si activation process in the subsequent cycles, implying that more Si reacts with lithium in each cycle.[42] Fig. 5c shows the galvanostatic charge and discharge profiles of the SiMP/CNT wrapping electrodes. The initial charge/discharge capacities of the SiMP/CNT wrapping 9 : 1 and SiMP/CNT wrapping 8 : 2 electrodes at 0.1 A g-1 are 3160.7 mA h g^{-1}/3469.1 mA h g^{-1} and 2376.6 mA h g^{-1}/2682.9 mA h g^{-1}, respectively. The corresponding initial coulombic efficiency of the SiMP/CNT wrapping 9 : 1 and SiMP/CNT wrapping 8 : 2 electrodes is 91.11 and 88.58%, respectively. Overall, the SiMP/CNT wrapping 9 : 1 electrode delivered a higher specific capacity with high ICE. The higher ICE of SiMP/CNT wrapping 9 : 1 could be due to the relatively lower surface area of the composite (Fig. 4d).[9,43] According to Fig. 4d, the BET surface area of SiMP/CNT wrapping 9 : 1 and SiMP/CNT wrapping 8 : 2 is 8.24 and 12.24 m^2 g^{-1}, respectively. The large surface area of the composite could result in increased electrolyte consumption and more SEI layer formation, resulting in low initial coulombic efficiency.[44–46] The result implies the superior electrochemical performance of the SiMP/CNT wrapping 9 : 1, even with a smaller amount of SWCNTs. The better electrochemical performance of the SiMP/CNT wrapping 9 : 1 electrode is attributed to the optimal structural properties of thin 2D SWCNT wrapping on the SiMPs. Compared to the dense and thick SWCNT layers in the SiMP/CNT wrapping 8 : 2 composite, the mesh-like CNT wrapping on the SiMPs and the porous SiMP/CNT wrapping 9 : 1 electrode structure could offer sufficient inner voids at the electrode level. This could be beneficial for facile lithium-ion diffusion.[40] As a result, we consider that the severe coverage derived from the larger amount of SWCNT dispersion in the SiMP/CNT wrapping 8 : 2 electrode could hamper the electrochemical activity of the SiMPs. In Fig. 5d, the rate performances of the SiMP/CNT wrapping electrodes at various C-rates are shown. The SiMP/CNT wrapping 9 : 1 electrode exhibits 3205.6, 3045.5, 2753.8, 2526.6, 2084.2, and 3173.3 mA h g^{-1} in the first step for each C-rate at 0.2, 0.5, 1.0, 1.5, 2.0, and 0.2 A g^{-1}. The SiMP/CNT wrapping 8 : 2 electrode delivers 2514.6, 2313, 2113.1, 1888, 1588.1, and 2557.4 mA h g^{-1} under the same conditions. The corresponding galvanostatic charge and discharge profiles at various C-rates for the SiMP/CNT wrapping 9 : 1 and 8 : 2 electrodes are shown in Fig. S7a and b†. Despite its relatively lower amount of SWCNTs, SiMP/CNT wrapping 9 : 1 exhibits higher specific capacities at the various C-rates, which is attributed to its optimal structural properties. Due to the efficient CNT wrapping, the electrical isolation of the SiMPs could be

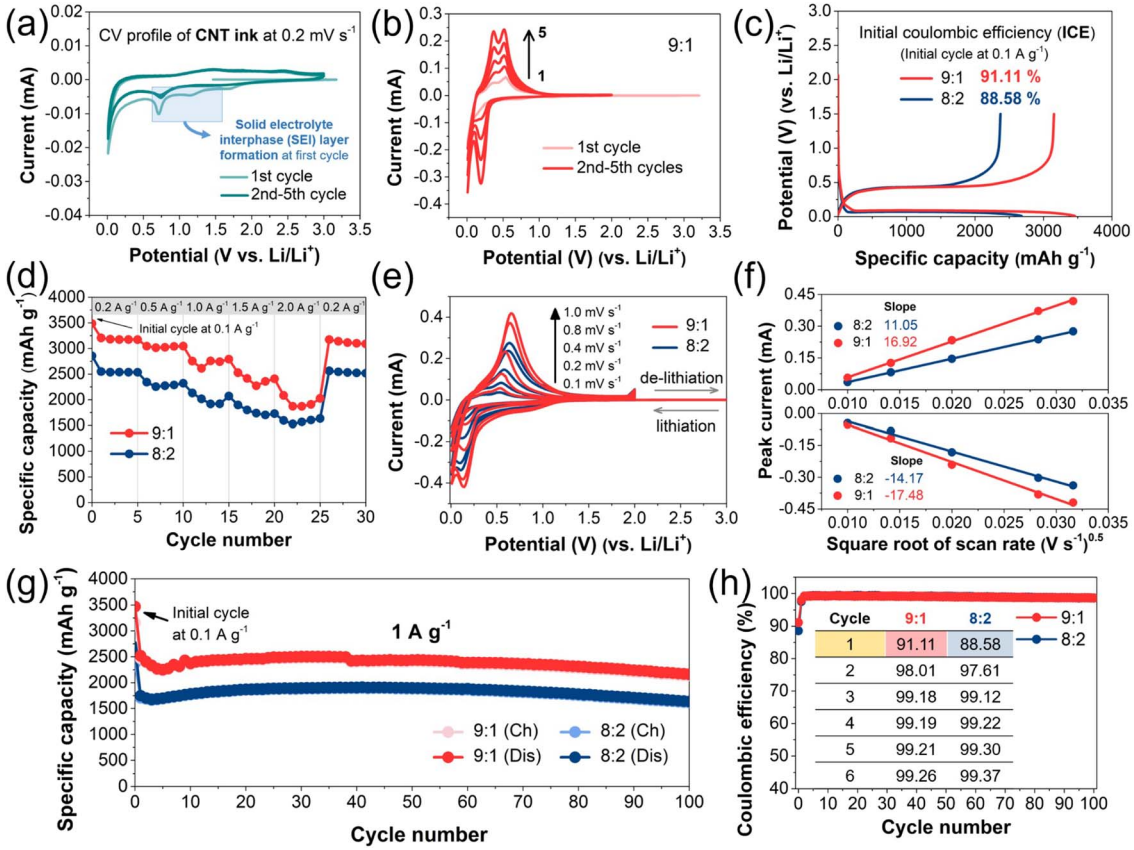

Fig. 5 (a) Cyclic voltammetry (CV) profile of CNT dispersion at a scan rate of 0.2 mV s^{-1} for 5 cycles. A semi-transparent blue box indicates the potential range of SEI layer formation in the first cycle. (b) CV profiles of SiMP/CNT wrapping 9 : 1 electrode at a scan rate of 0.2 mV s^{-1} for 5 cycles. (c) Galvanostatic charge and discharge profile of SiMP/CNT wrapping 8 : 2 and 9 : 1 electrodes with initial coulombic efficiencies (ICEs). (d) Rate performance of SiMP/CNT wrapping 8 : 2 and 9 : 1 electrodes at various C-rates from 0.2 to 2.0 A g^{-1}. (e) CV profiles of SiMP/CNT wrapping 8 : 2 and 9 : 1 electrodes at various scan rates from 0.1 to 1.0 mV s^{-1}. (f) Corresponding plot of the CV peak current of the anodic peak and cathodic peak against the square root of scan rate for the SiMP/CNT wrapping 8 : 2 and 9 : 1 electrodes. (g) Cycling performance of the SiMP/CNT wrapping 8 : 2 and 9 : 1 electrodes at 1.0 A g^{-1} for 100 cycles. (h) Corresponding coulombic efficiencies for the 1st and subsequent cycles.

effectively suppressed. SiMP/CNT wrapping 8 : 2 shows good rate capability at high current densities because of its larger amount of SWCNTs. Furthermore, the thick 2D CNT sheets in the SiMP/CNT wrapping 8 : 2 composite could ensure improved structural stability of the conductive network. As for the lower specific capacities of SiMP/CNT wrapping 8 : 2, we consider that the dense CNT coverage on the SiMP/CNT wrapping 8 : 2 electrode could reduce lithium-ion transport into the active materials, resulting in lower specific capacities (Fig. 5d). In this regard, SiMP/CNT wrapping 9 : 1 with a porous electrode structure provides the optimized conditions for electrochemical performance with facile lithium-ion access. To understand the better electrical performance of the SiMP/CNT wrapping 9 : 1 electrode, we investigated the kinetics of the SiMP/CNT wrapping composites. In Fig. 5e, the CV curves of the SiMP/CNT wrapping 9 : 1 and SiMP/CNT wrapping 8 : 2 electrodes at different scan rates (0.1–1.0 mV s^{-1}) are shown. As expected, the SiMP/CNT wrapping 9 : 1 electrode exhibits an increased magnitude of current response in the CV data compared to that of the SiMP/CNT wrapping 8 : 2 electrode. Interestingly, neither the SiMP/CNT wrapping 9 : 1 nor the SiMP/CNT wrapping 8 : 2 electrodes showed distinct anodic peaks at the various scan rates. We expect that this could be due to fast scan rate changes from 0.1 mV s^{-1} to 1.0 mV s^{-1}. These results have been observed in Si-based anode materials in other studies.[8,47,48] In addition, the small changes in the CV profiles and peak position deviation in Fig. 5e could be the result of electrochemical polarization.[49] The corresponding plots of the anodic and cathodic peak currents (I_p) against the square root of the scan rate of the SiMP/CNT wrapping 9 : 1 and SiMP/CNT wrapping 8 : 2 electrodes under different scan rates are shown in Fig. 5f. The redox kinetics of both electrodes are analyzed using the Randles–Sevcik eqn (1).[50]

$$I_p = (2.69 \times 10^5) n^{1.5} A D_{Li}^{0.5} v^{0.5} C_{Li^+} \quad (1)$$

In the equation, I_p, n, A, D_{Li}, v, and C_{Li^+} stand for the peak current, the number of transferred electrons, electrode surface area, diffusion coefficient, potential scanning rate, and lithium concentration in the electrolyte, respectively.[50] The results show a linear relationship between the peak currents and the square

root of scan rate (Fig. 5f). Based on the CV performance in Fig. 5e, we found that the SiMP/CNT wrapping 9 : 1 electrode exhibits better kinetics, implying the better electrochemical performance of SiMP/CNT wrapping 9 : 1. The cycling performance of the SiMP/CNT wrapping electrodes is shown in Fig. 5g. The SiMP/CNT wrapping 9 : 1 electrode exhibits higher specific capacities than that of the SiMP/CNT wrapping 8 : 2 electrode for 100 cycles. In the cycling performance of the SiMP/CNT wrapping 9 : 1 electrode, there are small capacity fluctuations, although this was not observed in the SiMP/CNT wrapping 8 : 2 electrode. This result implies that the higher content of SWCNTs in the SiMP/CNT wrapping 8 : 2 electrode ensures good structural stability. After 100 cycles, the SiMP/CNT wrapping 9 : 1 and SiMP/CNT wrapping 8 : 2 electrodes show capacity retention of 85.87 and 93.68%, respectively. In the SiMP/CNT wrapping composite, the SWCNTs, with superior mechanical stability, could ensure a stable structural network. Therefore, we consider that a larger amount of CNTs in the composite could improve the structural integrity against the volume changes of Si upon repeated charge and discharge cycling. According to previous studies, both initial and later-cycle coulombic efficiencies are regarded as important parameters for battery performance evaluation.[6,51] The corresponding coulombic efficiency trends of cycling performance are shown in Fig. 5h. With high initial coulombic efficiencies, the SiMP/CNT wrapping 9 : 1 and SiMP/CNT wrapping 8 : 2 composites exhibit good later-cycle coulombic efficiencies of almost 98–99%. The improvement of early- and later-cycle coulombic efficiencies could be affected by stable SEI formation. Furthermore, the robust 2D CNT wrapping on the SiMPs might prevent uncontrolled SEI formation derived from repeated Si pulverization during volume changes.[6] As a result, the SiMP/CNT wrapping 9 : 1 composite with thin 2D CNT wrapping exhibits high initial and later-cycle coulombic efficiencies along with stable SEI layer formation. In addition, a galvanostatic intermittent titration technique (GITT) test was conducted for the SiMP/CNT wrapping 9 : 1 and SiMP/CNT wrapping 8 : 2 electrodes (Fig. S8†).[3,8] According to Fig. S8a†, the SiMP/CNT wrapping 9 : 1 electrode had a lower overpotential than that of the SiMP/CNT wrapping 8 : 2 electrode, resulting in better dynamic behavior.[52–54] The magnified GITT profile in Fig. S8b† indicates lower polarization and internal resistance for the SiMP/CNT wrapping 9 : 1 electrode, which could be due to its optimal material and electrode structure.[52] The diffusion coefficient of Li^+ was calculated based on eqn (S1).† The lithium-ion diffusion kinetics of the SiMP/CNT wrapping 9 : 1 electrode are comparable to that of the SiMP/CNT wrapping 8 : 2 electrode (Fig. S8c†). The electrochemical performance of our work was further compared with other studies of SiMP/carbon composites in Table S1†. We found that the material in our work exhibits high initial capacities with superior ICE and comparable capacity retention due to efficient the SiMP/CNT wrapping composite structure.

To elucidate their electrochemical performance, electrochemical impedance spectroscopy (EIS) testing was conducted for the SiMP/CNT wrapping electrodes (Fig. 6a and b). In an attempt to prevent the influence of the lithium metal, each electrode was tested as a symmetric cell.[9,39,40] Both SiMP/CNT wrapping 9 : 1 and SiMP/CNT wrapping 8 : 2 electrodes were tested in a galvanostatic mode at 1 A g^{-1} for 20 cycles. After cycling, the resulting 20-cycle electrodes were prepared with a state-of-charge (SoC) of 50% because the lithiated state of Si could influence the internal resistance. The corresponding equivalent circuits are shown in Fig. 6c and d. In Fig. 6a, the SiMP/CNT wrapping 9 : 1 and SiMP/CNT wrapping 8 : 2 electrodes show comparable impedance spectra for the initial state. The parameters R_s, R_{SEI}, and R_{ct} correspond to solution resistance, SEI layer resistance, and charge-transfer resistance, respectively. We compared the Nyquist plots of the SiMP/CNT wrapping 9 : 1 and SiMP/CNT wrapping 8 : 2 electrodes in Fig. 6a and b. In the initial state before cycling, the R_s and R_{ct} of the SiMP/CNT wrapping 9 : 1 electrode are 3.40 $\pm$ 0.13 Ω and 3.01 $\pm$ 0.13 Ω, respectively (Fig. 6a). These parameters are smaller than those of the SiMP/CNT wrapping 8 : 2 electrode, which has an Rs and R_{ct} of 4.91 $\pm$ 0.04 Ω and 3.31 $\pm$ 0.04 Ω, respectively (Table S2†). The smaller internal resistance of the SiMP/CNT wrapping 9 : 1 electrode is attributed to the optimal structural properties of the composite and electrode. After 20 cycles, each electrode was assembled as a symmetric cell for EIS analysis. From Fig. 6b and Table S2†, the R_s, R_{SEI}, and R_{ct} of the SiMP/CNT wrapping 9 : 1 and SiMP/CNT wrapping 8 : 2 electrodes are 2.69 $\pm$ 0.38 Ω, 7.50 $\pm$ 4.57 Ω, and 22.67 $\pm$ 7.71 Ω and 5.01 $\pm$ 0.16 Ω, 14.45 $\pm$ 3.75 Ω, and 29.83 $\pm$ 14.05 Ω, respectively. The smaller internal resistances of the SiMP/CNT wrapping 9 : 1 electrode after 20 cycles are attributed to the stable SEI formation and optimal electrode structure. Furthermore, the evenly distributed conductive additive in the electrode with a hybrid conductive network could result in reduced resistance. Compared to the SiMP/CNT wrapping 9 : 1 electrode, the SiMP/CNT wrapping 8 : 2 electrode exhibits slightly larger internal resistances. To investigate the structural stability of the SiMP/CNT wrapping electrodes after cycling, we conducted SEM analysis on cycled electrodes (Fig. 6e–h).[55] Both the SiMP/CNT wrapping 9 : 1 and SiMP/CNT wrapping 8 : 2 electrodes exhibit smooth surfaces in Fig. 6e and g. As shown in Fig. 6g, the cycled SiMP/CNT wrapping 9 : 1 electrode shows a stable electrode surface. The well-preserved electrode structure was observed in a low-magnification SEM image. Therefore, we consider that the electrode was also preserved during repeated cycles. Interestingly, the high-magnification SEM images of the cycled electrodes show different structural properties (Fig. 6f and h). In the case of the SiMP/CNT wrapping 8 : 2 electrode, the cycled electrode shows thick SWCNT coverage on the SiMPs (Fig. 6f). Interestingly, the CNT networks are firmly attached to the SiMPs after cycling. In addition, the dense CNT-sheet-wrapped SiMPs are observed in the high-magnification SEM images of the cycled SiMP/CNT wrapping 8 : 2 electrode in Fig. 6f. The morphology of the SiMP/CNT wrapping 9 : 1 composite is also clearly shown in Fig. 6h. In the high-magnification SEM image, the morphology of the cycled SiMP/CNT wrapping 9 : 1 composite resembles insects captured by the lobes of a Venus flytrap. As the SWCNT sheets effectively wrap the silicon microparticles, the SiMPs could exhibit good electrochemical performance by taking advantage of the enhanced mechanical stability against Si volume changes and improved electrical

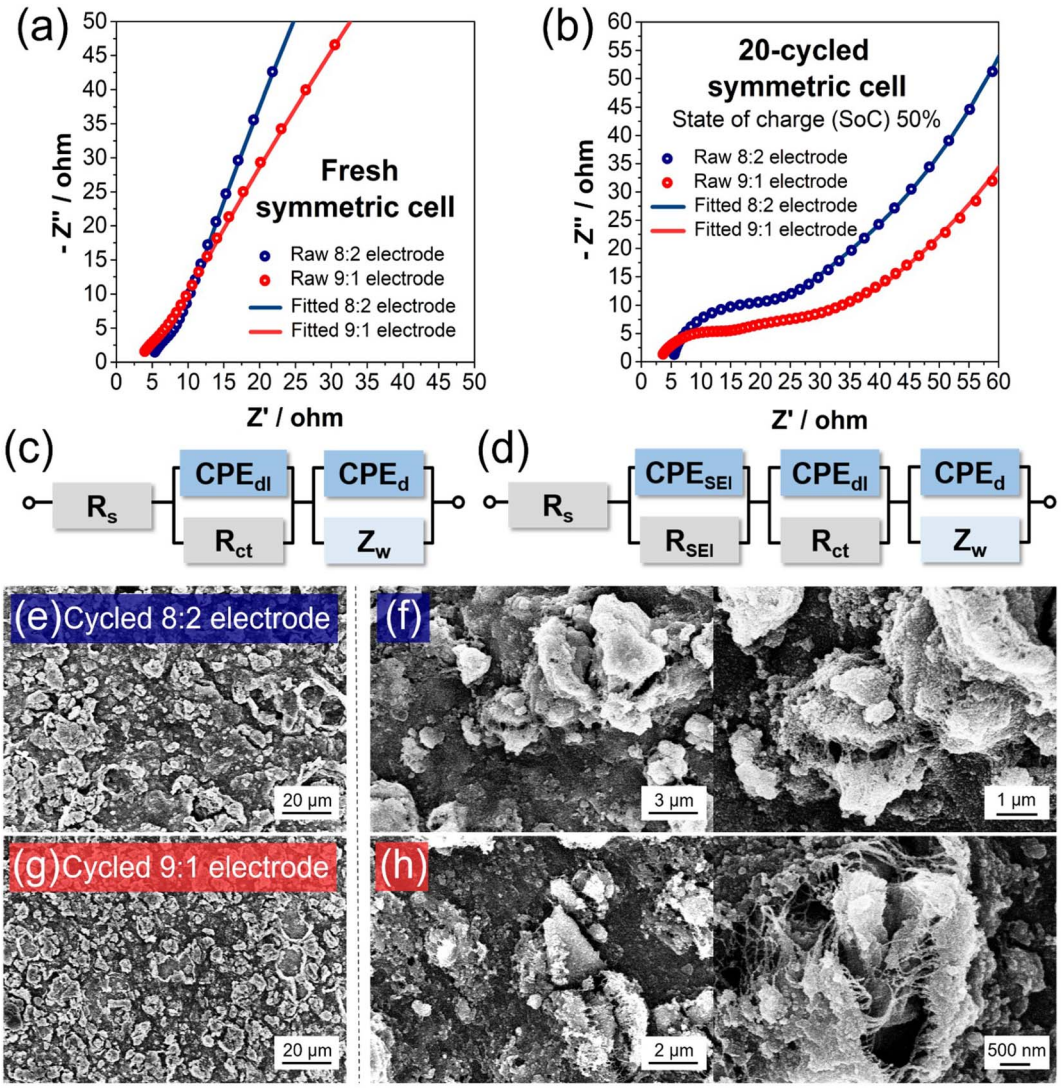

Fig. 6 Nyquist plots for a symmetric cells of the SiMP/CNT wrapping electrodes (a) before cycling and (b) after 20 cycles. The 20-cycled electrode was prepared with a state of charge (SoC) of 50%. Corresponding equivalent circuits (c) before and (d) after 20 cycles. Parameters in the equivalent circuit: R_s: contact resistance, R_{SEI}: SEI layer resistance, R_{ct}: charge transfer resistance, CPE_{dl}: double-layer capacitance, CPE_d: capacitance of solid-state diffusion, CPE_{SEI}: SEI layer capacitance, and Z_w: Warburg diffusion element of solid-state diffusion. SEM images of 20-cycled SiMP/CNT wrapping 8 : 2 electrode at (e) low and (f) high magnification. SEM images of 20-cycled SiMP/CNT wrapping 9 : 1 electrode at (g) low and (h) high magnification.

conductivity. Due to the efficient 2D CNT sheet wrapping structure using well-dispersed SWCNTs, the silicon microparticles could maintain electrochemical activity during cycling without electrical isolation or detachment from the electrode (Fig. 7a).[6] In Fig. 7b–e, TEM images of cycled SiMP/CNT wrapping electrodes are shown. For the cycled SiMP/CNT wrapping 8 : 2 electrode, dense and thick 2D CNT sheet coverage of the SiMPs is observed (Fig. 7b–c). In contrast, the cycled SiMP/CNT wrapping 9 : 1 electrode shows relatively thinner 2D CNT sheets due to the lower amount of SWCNT dispersion used for fabrication (Fig. 7d and e). After repeated cycling, the CNT wrapping is still seen in the TEM images, proving the excellent structural integrity of the CNT network. Furthermore, the embedded silicon microparticles in the SiMP/CNT wrapping composite are observed, indicating the efficient structural stability and conductive network in the composite. In Fig. S9a and b†, the magnified TEM images show the surface of the cycled SiMP/CNT wrapping 8 : 2 and SiMP/CNT wrapping 9 : 1 active material. We consider that the SEI layer is mainly expected to form on the 2D CNTs, which is the outer surface of the SiMP/CNT wrapping composites. Therefore, the SEI layer formation on the CNTs could result in high initial coulombic efficiency with a stable SEI layer.[6,51] In addition, the robust CNT wrapping could prevent uncontrolled SEI layer formation upon repeated pulverization of the SiMPs. Compared to that in Fig. S9b†, the magnified TEM image of cycled SiMP/CNT wrapping 8 : 2 in Fig. S9a† shows a thicker SEI layer. This could be due to the

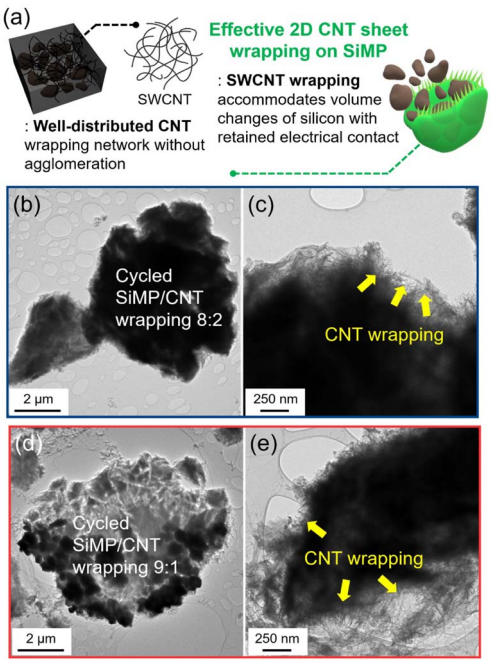

Fig. 7 (a) Schematic illustration of the SiMP/CNT wrapping composite after cycling. HR-TEM images of the SiMP/CNT wrapping 8 : 2 composite in the cycled electrode at (b) low and (c) high magnification. HR-TEM images of the SiMP/CNT wrapping 9 : 1 composite in the cycled electrode at (d) low and (e) high magnification.

larger surface area of the SiMP/CNT wrapping 8 : 2 composite (Fig. 4d).

4. Conclusions

In summary, we synthesized SiMP/CNT wrapping composites *via* freeze-drying using highly dispersed SWCNTs. While CNTs exhibit intrinsic drawbacks such as entanglement and agglomeration, in the composites, the well-dispersed CNTs were easily mixed with SiMPs, promoting effective wrapping on the SiMP surfaces. During lyophilization, the highly dispersed SWCNTs were simply self-assembled into mesh-like 2D CNT sheets *via* interactions among the CNTs. The wide-ranging CNT wrapping in the composite enabled it to effectively dissipate the volume expansion of Si and maintain electrical conductivity upon repeated cycles. The optimized SiMP/CNT wrapping 9 : 1 electrode delivered a superior ICE of 91.11% with a high charge and discharge capacity of 3160.7 mA h g^{-1} and 3469.1 mA h g^{-1} at 0.1 A g^{-1}, respectively. Furthermore, the SiMP/CNT wrapping 9 : 1 electrode exhibited good rate and cycle performance with high capacities and stable coulombic efficiencies during repeated charge and discharge. The thin 2D CNT sheet wrapping on the SiMPs effectively enhances mechanical stability, prevents continuous SEI formation, and preserves electrical conductivity. Furthermore, the mesh-like thin CNT sheets in the SiMP/CNT wrapping 9 : 1 composite would be beneficial for facile lithium-ion diffusion while maintaining a porous conducting network within the electrode, resulting in good electrochemical performance. This study suggests a useful guide for Si/CNT composite preparation. It can provide a promising approach for efficient CNT-based composite design for numerous applications.

Author contributions

Youngseul Cho: conceptualization, data curation, formal analysis, investigation, methodology, validation, visualization, writing – original draft. Kyu Sang Lee: methodology and formal analysis. Shuqing Piao: formal analysis. Taek-Gyoung Kim: formal analysis, investigation, and methodology. Seong-Kyun Kang: formal analysis and methodology. Sang Yoon Park: funding acquisition and project administration. Kwanghyun Yoo: supervision and project administration. Yuanzhe Piao: funding acquisition, supervision, and project administration.

Conflicts of interest

There are no conflicts to declare.

Acknowledgements

This research was supported by Basic Science Research Program through the National Research Foundation of Korea (NRF) funded by the Ministry of Education (NRF-2021R1A2C1008380), and the Nano Material Technology Development Program through the NRF funded by the Ministry of Science and ICT (NRF-2015M3A7B6027970 and NRF-2018M3A7B4070990). In addition, this research was partly supported by the Korea Institute of Energy Technology Evaluation and Planning (KETEP) funded by the Korea government (MOTIE) (20215710100170). This research was also supported by the Materials, Components & Equipment Research Program funded by the Gyeonggi Province.

Notes and references

1 J. W. Choi and D. Aurbach, *Nat. Rev. Mater.*, 2016, **1**, 16013.
2 S. Chae, M. Ko, K. Kim, K. Ahn and J. Cho, *Joule*, 2017, **1**, 47–60.
3 H. J. Kwon, J. Y. Hwang, H. J. Shin, M. G. Jeong, K. Y. Chung, Y. K. Sun and H. G. Jung, *Nano Lett.*, 2020, **20**, 625–635.
4 G. Song, M. J. Kwak, C. Hwang, C. An, S. Kim, S. Lee, S. Choi, H. K. Song, J. H. Jang and S. Park, *ACS Appl. Energy Mater.*, 2021, **4**, 10050–10058.
5 G. J. Zhu, D. L. Chao, W. L. Xu, M. H. Wu and H. J. Zhang, *ACS Nano*, 2021, **15**, 15567–15593.
6 Y. Z. Li, K. Yan, H. W. Lee, Z. D. Lu, N. Liu and Y. Cui, *Nat. Energy*, 2016, **1**, 15029.
7 Y. Y. Liu, G. M. Zhou, K. Liu and Y. Cui, *Acc. Chem. Res.*, 2017, **50**, 2895–2905.
8 P. Li, J. Y. Hwang and Y. K. Sun, *ACS Nano*, 2019, **13**, 2624–2633.
9 J. M. Kim, V. Guccini, D. Kim, J. Oh, S. Park, Y. Jeon, T. Hwang, G. Salazar-Alvarez and Y. Z. Piao, *J. Mater. Chem. A*, 2018, **6**, 12475–12483.

10 H. W. Wang, J. Z. Fu, C. Wang, J. Y. Wang, A. K. Yang, C. C. Li, Q. F. Sun, Y. Cui and H. Q. Li, *Energy Environ. Sci.*, 2020, **13**, 848–858.
11 B. M. Hu, X. L. Kuang, S. X. Xu and X. H. Wang, *Energy Technol.*, 2019, **7**, 1801047.
12 S. Zhu and J. F. Ni, *Chem. Rec.*, 2022, **22**, e202200125.
13 Y. Z. Wu, X. W. Zhao, Y. Y. Shang, S. L. Chang, L. X. Dai and A. Y. Cao, *ACS Nano*, 2021, **15**, 7946–7974.
14 S. H. Park, P. J. King, R. Y. Tian, C. S. Boland, J. Coelho, C. F. Zhang, P. McBean, N. McEvoy, M. P. Kremer, D. Daly, J. N. Coleman and V. Nicolosi, *Nat. Energy*, 2019, **4**, 560–567.
15 W. X. Ji, H. N. Qu, X. X. Zhang, D. Zheng and D. Y. Qu, *Small Methods*, 2021, **5**, 2100518.
16 L. F. Cui, L. B. Hu, J. W. Choi and Y. Cui, *ACS Nano*, 2010, **4**, 3671–3678.
17 J. H. Xu, Q. Y. Yin, X. R. Li, X. Y. Tan, Q. Liu, X. Lu, B. C. Cao, X. T. Yuan, Y. Z. Li, L. Shen and Y. F. Lu, *Nano Lett.*, 2022, **22**, 3054–3061.
18 W. S. Kim, J. Choi and S. H. Hong, *Nano Res.*, 2016, **9**, 2174–2181.
19 K. Fu, O. Yildiz, H. Bhanushali, Y. X. Wang, K. Stano, L. G. Xue, X. W. Zhang and P. D. Bradford, *Adv. Mater.*, 2013, **25**, 5109–5114.
20 J. M. Kim, V. Guccini, K. D. Seong, J. Oh, G. Salazar-Alvarez and Y. Piao, *Carbon*, 2017, **118**, 8–17.
21 Y. Surace, M. Simoes, L. Karvonen, S. Yoon, S. Pokrant and A. Weidenkaff, *J. Alloys Compd.*, 2015, **644**, 297–303.
22 S. Kang, S. Y. Hong, N. Kim, J. Oh, M. Park, K. Y. Chung, S. S. Lee, J. Lee and J. G. Son, *ACS Nano*, 2020, **14**, 3660–3668.
23 X. S. Zhou, Y. X. Yin, L. J. Wan and Y. G. Guo, *Chem. Commun.*, 2012, **48**, 2198–2200.
24 J. Q. Han, C. J. Zhou, Y. Q. Wu, F. Y. Liu and Q. L. Wu, *Biomacromolecules*, 2013, **14**, 1529–1540.
25 Y. Ma, R. Younesi, R. J. Pan, C. J. Liu, J. F. Zhu, B. Q. Wei and K. Edstrom, *Adv. Funct. Mater.*, 2016, **26**, 6797–6806.
26 H. L. Zhang, L. H. Xu, F. Y. Yang and L. Geng, *Carbon*, 2010, **48**, 688–695.
27 J. Santos, A. Silva and R. Bretas, *AIP Conf. Proc.*, 2015, **1664**, 070021.
28 P. C. Ma, N. A. Siddiqui, G. Marom and J. K. Kim, *Composites, Part A*, 2010, **41**, 1345–1367.
29 Y. Y. Huang and E. M. Terentjev, *Polymers*, 2012, **4**, 275–295.
30 X. Zhang, Z. Y. Ju, L. M. Housel, L. Wang, Y. Zhu, G. Singh, N. Sadique, K. J. Takeuchi, E. S. Takeuchi, A. C. Marschilok and G. H. Yu, *Nano Lett.*, 2019, **19**, 8255–8261.
31 R. E. Ruther, K. A. Hays, S. J. An, J. L. Li, D. L. Wood and J. Nanda, *ACS Appl. Mater. Interfaces*, 2018, **10**, 18641–18649.
32 Z. F. Liu, J. Zhang and B. Gao, *Chem. Commun.*, 2009, 6902–6918.
33 H. Telg, J. G. Duque, M. Staiger, X. M. Tu, F. Hennrich, M. M. Kappes, M. Zheng, J. Maultzsch, C. Thomsen and S. K. Doorn, *ACS Nano*, 2012, **6**, 904–911.
34 X. H. Li, M. Q. Wu, T. T. Feng, Z. Q. Xu, J. G. Qin, C. Chen, C. Y. Tu and D. X. Wang, *RSC Adv.*, 2017, **7**, 48286–48293.
35 S. Y. Chew, S. H. Ng, J. Z. Wang, P. Novak, F. Krumeich, S. L. Chou, J. Chen and H. K. Liu, *Carbon*, 2009, **47**, 2976–2983.
36 Z. Y. Zhang, Z. W. Li, Q. Luo, B. Z. Yang, Y. Liu, Y. Y. Hu, X. B. Liu, Y. H. Yin, Y. S. Li and Z. P. Wu, *Carbon*, 2022, **188**, 238–245.
37 C. L. Li, C. Liu, K. Ahmed, Z. Mutlu, Y. Yan, I. Lee, M. Ozkan and C. S. Ozkan, *RSC Adv.*, 2017, **7**, 36541–36549.
38 J. L. Zhu, Y. R. Ren, B. Yang, W. K. Chen and J. N. Ding, *Nanoscale Res. Lett.*, 2017, **12**, 627.
39 J. M. Kim, Y. Cho, V. Guccini, M. Hahn, B. Y. Yan, G. Salazar-Alvarez and Y. Piao, *Electrochim. Acta*, 2021, **369**, 137708.
40 Y. Cho, J. M. Kim, B. Y. Yan, H. Hong and Y. Piao, *J. Electroanal. Chem.*, 2020, **876**, 114475.
41 M. Choi, J. C. Kim and D. W. Kim, *Sci. Rep.*, 2018, **8**, 960.
42 C. K. Chan, H. L. Peng, G. Liu, K. McIlwrath, X. F. Zhang, R. A. Huggins and Y. Cui, *Nat. Nanotechnol.*, 2008, **3**, 31–35.
43 M. S. Kang, I. Heo, S. Kim, J. Yang, J. Kim, S. J. Min, J. Chae and W. C. Yoo, *Energy Storage Mater.*, 2022, **50**, 234–242.
44 X. H. Zhang, R. Y. Guo, X. L. Li and L. J. Zhi, *Small*, 2018, **14**, 1800752.
45 H. Gao, L. S. Xiao, I. Plume, G. L. Xu, Y. Ren, X. B. Zuo, Y. Z. Liu, C. Schulz, H. Wiggers, K. Amine and Z. H. Chen, *Nano Lett.*, 2017, **17**, 1512–1519.
46 Y. C. Mo, S. C. Li and J. Yu, *ACS Appl. Nano Mater.*, 2022, **5**, 8205–8213.
47 M. T. Xia, B. J. Chen, F. Gu, L. H. Zu, M. Z. Xu, Y. T. Feng, Z. J. Wang, H. J. Zhang, C. Zhang and J. H. Yang, *ACS Nano*, 2020, **14**, 5111–5120.
48 X. Wan, T. S. Mu, B. C. Shen, Q. Meng, G. C. Lu, S. F. Lou, P. J. Zuo, Y. L. Ma, C. Y. Du and G. P. Yin, *Nano Energy*, 2022, **99**, 107334.
49 X. J. Xu, F. Z. Wu, W. L. Yang, X. Y. Dai, T. H. Wang, J. W. Zhou, J. Wang and D. Guo, *ACS Sustainable Chem. Eng.*, 2021, **9**, 13215–13224.
50 L. L. Hu, M. H. Jin, Z. Zhang, H. X. Chen, F. B. Ajdari and J. X. Song, *Adv. Funct. Mater.*, 2022, **32**, 2111560.
51 J. Y. Wang, L. Liao, H. R. Lee, F. F. Shi, W. Huang, J. Zhao, A. Pei, J. Tang, X. L. Zheng, W. Chen and Y. Cui, *Nano Energy*, 2019, **61**, 404–410.
52 C. H. Jung, K. H. Kim and S. H. Hong, *J. Mater. Chem. A*, 2019, **7**, 12763–12772.
53 Z. Zhang, F. S. Xi, X. H. Chen, S. Y. Li, W. H. Ma, Z. Ding, T. Qu, Y. N. Dai and R. Deng, *Environ. Chem. Lett.*, 2022, **20**, 3377–3385.
54 T. Meng, B. Li, C. Liu, Q. S. Wang, H. J. Su, L. Hu, J. N. Hao, E. P. Du, F. L. Gu, B. B. Huang, J. D. Yang and Y. X. Tong, *Cell Rep. Phys. Sci.*, 2021, **2**, 100486.
55 Y. K. Jeong, T. W. Kwon, I. Lee, T. S. Kim, A. Coskun and J. W. Choi, *Energy Environ. Sci.*, 2015, **8**, 1224–1230.